

Accepted Manuscript

Synthesis and molecular structures of the 52-electron triiron telluride clusters
[Fe₃(CO)₈(μ₃-Te)₂(κ²-diphosphine)] - Electrochemical properties and activity as
proton reduction catalysts

Ahibur Rahaman, George C. Lisensky, Derek A. Tocher, Michael G. Richmond,
Graeme Hogarth, Ebbe Nordlander

PII: S0022-328X(18)30209-2

DOI: [10.1016/j.jorganchem.2018.03.038](https://doi.org/10.1016/j.jorganchem.2018.03.038)

Reference: JOM 20388

To appear in: *Journal of Organometallic Chemistry*

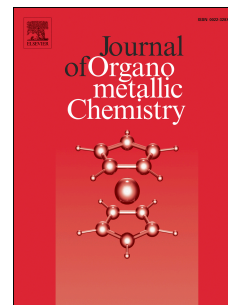
Received Date: 12 February 2018

Revised Date: 25 March 2018

Accepted Date: 26 March 2018

Please cite this article as: A. Rahaman, G.C. Lisensky, D.A. Tocher, M.G. Richmond, G. Hogarth, E. Nordlander, Synthesis and molecular structures of the 52-electron triiron telluride clusters [Fe₃(CO)₈(μ₃-Te)₂(κ²-diphosphine)] - Electrochemical properties and activity as proton reduction catalysts, *Journal of Organometallic Chemistry* (2018), doi: 10.1016/j.jorganchem.2018.03.038.

This is a PDF file of an unedited manuscript that has been accepted for publication. As a service to our customers we are providing this early version of the manuscript. The manuscript will undergo copyediting, typesetting, and review of the resulting proof before it is published in its final form. Please note that during the production process errors may be discovered which could affect the content, and all legal disclaimers that apply to the journal pertain.



Synthesis and molecular structures of the 52-electron triiron telluride clusters $[\text{Fe}_3(\text{CO})_8(\mu_3\text{-Te})_2(\kappa^2\text{-diphosphine})]$ - electrochemical properties and activity as proton reduction catalysts

Ahibur Rahaman,^a George C. Lisensky,^b Derek A. Tocher,^c Michael G. Richmond,^d Graeme Hogarth^{*e} and Ebbe Nordlander^{*a}

^a*Chemical Physics, Department of Chemistry, Lund University, Box 124, SE-221 00 Lund, Sweden*

^b*Department of Chemistry, Beloit College, Beloit, WI 53511, USA*

^c*Department of Chemistry, University College London, 20 Gordon Street, London WC1H 0AJ, UK*

^d*Department of Chemistry, University of North Texas, 1155 Union Circle, Box 305070, Denton, Texas 76203, USA*

^e*Department of Chemistry, King's College London, Britannia House, 7 Trinity Street, London SE1 1DB, UK*

Dedicated to Prof. Irina P. Beletskaya on her 85th birthday, and in recognition of her outstanding contributions to organometallic chemistry.

Abstract – Heating the 50-electron cluster $[\text{Fe}_3(\text{CO})_9(\mu_3\text{-Te})_2]$ (**1**) with the diphosphines $\text{Ph}_2\text{P-R-PPh}_2$ [$\text{R} = -\text{CH}_2\text{CH}_2-$ (dppe), Z-CH=CH- (dppv), $1,2\text{-C}_6\text{H}_4$ (dppb), $-\text{CH}_2\text{CH}_2\text{CH}_2-$ (dppp), ferrocenyl (dppf), naphthalenyl (dppbn)] in benzene affords the 52-electron diphosphine-containing tellurium-capped triiron clusters $[\text{Fe}_3(\text{CO})_8(\mu_3\text{-Te})_2(\kappa^2\text{-diphosphine})]$ (diphosphine = dppe, dppv, dppb, dppp, dppf, dppnd) (**2-7**) in moderate yields, resulting from both phosphine addition and carbonyl loss. With 1,2-bis(diphenylphosphino) benzene (dppb) a second product is the cubane cluster $[\text{Fe}_4(\text{CO})_{10}(\mu_3\text{-Te})_4(\kappa^2\text{-dppb})]$ (**8**). Cyclic voltammetry measurements on **2-7** reveals that all clusters show irreversible reductive behaviour at ca. -1.85 V with a series of associated small back oxidation waves, suggesting that reduction leads to significant structural change but that this can be reversed chemically. Oxidation occurs at relatively low potentials and is diphosphine-dependent. The first oxidation appears at ca. +0.35 V for **2-6** with a small degree of reversibility but is as low as +0.14 V for the bis(diphenylphosphino)naphthalene derivative **7** and in some cases is followed by further closely-spaced oxidation. Addition of $[\text{Cp}_2\text{Fe}][\text{PF}_6]$ to **2-7** results in the formation of new clusters formulated as $[\text{Fe}_3(\text{CO})_8(\mu_3\text{-Te})_2(\kappa^2\text{-diphosphine})]^+$, with their IR spectra suggesting oxidation at the diiron centre. This is supported by computational studies (DFT) of the bis(diphenylphosphino)propane cluster **5** showing that the HOMO is the Fe-Fe σ -bonding orbital, while the LUMO is centered on the diphosphine-substituted iron atom and has significant Fe-Te σ^* -anti-bonding character consistent with the irreversible nature of the reduction. Complexes **2-7** have been examined as proton reduction catalysts in the presence of *para*-toluenesulfonic acid (TsOH). All are active at their first reduction potential, with a second catalytic process being observed at slightly higher potentials. While their overall electrocatalytic behaviour is similar to that noted for the $[\text{Fe}_2(\text{CO})_6\{\mu\text{-E}(\text{CH}_2)_3\text{E}\}]$ (E = S, Se, Te), the DFT results suggest that as the added electron is localised on the unique iron atom, the mechanistic aspects of hydrogen formation are likely to be quite different from the more widely studied diiron models.

Keywords: iron, tellurium, diphosphine, electrochemistry, proton reduction

1. Introduction

Dithiolate-bridged diiron complexes that mimic the active site of [FeFe]-hydrogenases have been widely studied as proton reduction catalysts over the past 15 years [1-8]. In the very effective so called [FeFe]-hydrogenases only sulfur-containing ligands are found, but in some related [FeNi]-hydrogenases, sulfur is replaced by selenium and this leads to greater oxidative stability [9]. While levels of tellurium in living systems are similar to those of selenium, to date no biological use of this heavy chalcogenide have been identified [10]. A key feature of an active biomimic of a hydrogenase is their ability to operate at low overpotentials [2-7]. Weigand and co-workers have reported that the replacement of sulfur in the well-studied hydrogenase biomimic $[\text{Fe}_2(\text{CO})_6\{\text{E}(\text{CH}_2)_3\text{E}\}]$ ($\text{E} = \text{S}$) (Fig 1a) [6], with selenium or tellurium results in a decrease in the first reduction potential in the order $\text{S} > \text{Se} > \text{Te}$ [6]. Such a reduction is important to the activation of the complexes as proton reduction catalysts and thus suggests that iron-tellurium complexes could be potentially useful catalysts in this respect. Tellurium-containing clusters have attracted interest as a result of their novel structural features and unusual reactivity patterns [11-34].

A further development of [FeFe]-hydrogenase biomimics has been to replace the organic dithiolate linking group with a metal fragment (Fig. 1b), with examples containing nickel and platinum being widely studied [35-40]. A large number of transition metal chalcogenide complexes of high nuclearity (three or more transition metals) containing phosphine ligands has been synthesised and structurally characterized [11-33], but to our knowledge none have been studied as proton reduction catalysts. Considering the results obtained by Weigand and coworkers [6] and the potential adventitious inclusion of a third metal center, we targeted triiron-tellurium complexes (Fig. 1c) as potential proton reduction catalysts. Here we report the synthesis, structural characterization and electrochemical behaviour of the 52-electron diphosphine-containing tellurium-capped triiron clusters $[\text{Fe}_3(\text{CO})_8(\mu_3\text{-Te})_2(\kappa^2\text{-diphosphine})]$ (diphosphine = dppe, dppv, dppb, dppp, dppf, dppnd) (**2-7**) (Fig. 1c). During the course of these studies we also isolated the new cubane cluster, $[\text{Fe}_4(\text{CO})_{10}(\mu_3\text{-Te})_4(\kappa^2\text{-dppb})]$ (**8**), the structure of which has been determined. We have carried out electrochemical studies on **2-7**, the results of which are supported by DFT calculations, and in preliminary studies show them to be catalysts for electrochemical reduction of protons in the presence of *para*-toluenesulfonic acid (TsOH).

insert Fig. 1 near here

2. Results and discussion

2.1. Synthesis of $[Fe_3(CO)_8(\mu_3-Te)_2(\kappa^2\text{-diphosphine})]$ (2-7)

The parent 50-electron cluster $[Fe_3(CO)_9(\mu_3-Te)_2]$ (**1**) was synthesised as previously reported [23]. Heating **1** in benzene with a range of bidentate phosphines $Ph_2P\text{-R-}PPh_2$ [R = $-\text{CH}_2\text{CH}_2-$ (dppe), $Z\text{-CH=CH-}$ (dppv), $1,2\text{-C}_6\text{H}_4$ (dppb), $-\text{CH}_2\text{CH}_2\text{CH}_2-$ (dppp), ferrocenyl (dppf), naphthalenyl (dppbn)] with a tendency to chelate (Scheme 1) gave the new 52-electron clusters $[Fe_3(CO)_8(\mu_3-Te)_2(\kappa^2\text{-}Ph_2PRPPH_2)]$ (2-7) in yields ranging from 10-60% as the major reaction product. The 1,2-bis(diphenylphosphino)ethane (dppe) derivative **2** and the analogous cluster $[Fe_3(CO)_8(\mu_3-Te)_2(\kappa^2\text{-dppm})]$ have been reported previously [12,39a], being formed upon addition of dppe to $[Fe_3(CO)_8(PPh_3)(\mu_3-Te)_2]$ at room temperature [12] or by addition of the relevant diphosphine (dppm, dppe) to **1** to form $[Fe_3(CO)_9(\mu_3-Te)_2(\kappa^1\text{-diphosphine})]$ (diphosphine coordinated in “dangling mode” (*vide infra*)) followed by heating in benzene [39a]. Furthermore, the reaction of **1** with triphenylarsine, triphenylphosphite or phosphines leads to the related $[Fe_3(CO)_9(\mu_3-Te)_2(L)]$ clusters [27,39a] and the parent complex $[Fe_3(CO)_{10}(\mu_3-Te)_2]$, which has been structurally characterized [41], is formed upon the reaction of **1** with carbon monoxide [27]. Interestingly, addition of dppe to **1** (in a 1:2 ratio) at room temperature is reported to yield the diphosphine-linked hexa-iron cluster $[{Fe_3(CO)_8(\mu_3-Te)_2}_2(\kappa^2\text{-dppe})]$ which has been crystallographically characterised [12]. It is not clear whether this is an intermediate in the formation of **2**. The preparation of the 1,1'-bis(diphenylphosphino)ferrocene (dppf) derivative **6** in 72% yield from the reaction of **1** and dppf in CH_2Cl_2 at room temperature has also been reported [42]. All new clusters were characterised spectroscopically. For each compound, the carbonyl region of the IR spectrum exhibited four bands in a distinctive and characteristic pattern, for example at 2038s, 1995vs, 1960s, 1951m cm^{-1} for the 1,3-bis(diphenylphosphino)propane (dppp) analogue **5**. The equivalence of the two phosphorus atoms was also clearly shown in the $^{31}P\{^1H\}$ NMR spectrum by the appearance of a singlet resonance (at 42.0 ppm for **5**).

insert Scheme 1 near here

2.2. Molecular structures of $[Fe_3(CO)_8(\mu_3-Te)_2(\kappa^2\text{-diphosphine})]$ (4,5,7)

The molecular structures of **4**, **5** and **7** have been determined by single crystal X-ray diffraction and the results are depicted in Figure 2. Important metric parameters for the three compounds and related chalcogenide-capped clusters are summarised in Table 1, and selected bond lengths and bond angles are collated in Table 2. Each cluster contains a triiron core capped by two triply bridging tellurium ligands, and contains a single iron-iron bond (Fe-Fe 2.583(5)-2.601(5) Å). The diphosphine chelates to the unique iron atom with P-Fe-P bond angles of 87.25(2)°, 94.12(3)°, and 97.70(9)° in **4**, **5** and **7**, respectively, which are close to that of 88.34(14)° found in **2** [12]. This iron atom is also ligated by two terminal carbonyls in a relative *trans* disposition. The Te-Te distances, ranging from 3.107(3)-3.152(2) Å in **4**, **5** and **7**, are quite short but similar to that of 3.138(1) Å found in [Fe₃(CO)₉(μ₃-Te)₂(PPh₃)] [39a], and do not represent a formal Te-Te bond.

insert Fig. 2 near here

With dppf and dppbn, a second product was isolated, but they remain to be fully identified. For both products, their IR spectra displayed four ν_{C-O} bands (e.g. at 2063w, 2040vs, 2002s and 1970m cm⁻¹ for the dppbn derivative) that are shifted to higher frequencies than those in **2-7**. Chatterjee and coworkers prepared [Fe₃(CO)₉(μ₃-Te)₂(κ¹-dppf)], with the dppf ligand in a monodentate “dangling” coordination mode, from the reaction of **1** with dppf at -10 °C [42] and Rauchfuss and coworkers identified the clusters [Fe₃(CO)₉(μ₃-Te)₂(κ¹-diphosphine)] (diphosphine=dppm, dppe) [39a]. The cluster [Fe₃(CO)₉(μ₃-Te)₂(κ¹-dppf)] exhibits two singlets at 28.0 and -18.0 ppm in its ³¹P{¹H} NMR spectrum. The IR spectra of our minor dppf and dppbn products and [Fe₃(CO)₉(μ₃-Te)₂(κ¹-dppf)] are identical, but the ³¹P{¹H} NMR spectrum of the minor dppf product reveals two high field resonances at 51.0 and 28.0 ppm, consistent with oxidation of the pendant phosphorus atom. Thus, we *tentatively* identify this minor product as [Fe₃(CO)₉(μ₃-Te)₂(κ¹-dppfO)]. We note, in passing, that the analogous compound [Fe₃(CO)₉(μ₃-Te)₂(κ¹-dppeS)], prepared by reaction of [Fe₃(CO)₉(μ₃-Te)₂(κ¹-dppe)] with sulfur, has been characterized by IR and NMR spectroscopies [39a].

2.3. Molecular structure of [Fe₄(CO)₁₀(μ₃-Te₄)(κ²-dppb)] (**8**)

With 1,2-bis(diphenylphosphino)benzene (dppb), a second product was isolated and identified as the cubane cluster [Fe₄(CO)₁₀(μ₃-Te₄)(κ²-dppb)] (**8**), which was formed in 12% yield. The spectroscopic data are in full accord with this formulation, and X-ray crystallography was used to elucidate the structure (Figure 3). Selected bond lengths and

angles being given in Tables S1 (Supplementary Information). The cluster has a Te_4Fe_4 cubane core, with alternating tellurium and iron atoms. Each telluride is thus triply bridging and there are no formal metal-metal bonds. Three of the iron atoms are ligated by three carbonyl ligands, while the fourth has a single carbonyl and the chelating diphosphine ligand. It is a derivative of the parent cluster $[\text{Fe}_4(\text{CO})_{12}(\mu_3\text{-Te})_4]$, which has been prepared by Rauchfuss and co-workers by irradiation of $[\text{Fe}_2(\text{CO})_6(\mu_2\text{-Te}_2)]$ [40b]. The related bis(diphenylphosphino)methane (dppm) derivative, $[\text{Fe}_4(\text{CO})_{10}(\mu_3\text{-Te})_4(\mu\text{-dppm})]$, has also been reported, resulting from the unusual reaction of $[\text{NMe}_4]_2[\text{Te}_{10}\text{Fe}_8(\text{CO})_{28}]$ (which consists of two Fe_4Te_4 cubane clusters linked by a Te_2 moiety) with $[\text{Cu}_2(\mu\text{-dppm})_2(\text{MeCN})_4][\text{BF}_4]_2$ [43]. In the dppm derivative the diphosphine bridges an iron-iron vector, in contrast to **8** where it chelates to a single iron center. The average Te-Fe bond length in **8** of 2.625 Å is similar to those in related Fe_4Te_4 clusters [43-46] and the Fe-Te-Fe bond angles $[94.50(2)\text{-}98.47(2)^\circ]$ and Te-Fe-Te bonds angles $[81.02(1)\text{-}83.83(1)^\circ]$ are within expected ranges.

Insert Fig 3 and Tables 1 and 2 near here

The mode of formation of **8** is unclear. Rauchfuss and coworkers have previously noted that thermal degradation of **1** affords $[\text{Fe}_2(\text{CO})_6(\mu\text{-Te}_2)]$, which in turn can dimerise to give $[\text{Fe}_4(\text{CO})_{12}(\mu_3\text{-Te})_4]$ [40b]. Hence **8** may simply arise as a result of the *in situ* carbonyl substitution of $[\text{Fe}_4(\text{CO})_{12}(\mu_3\text{-Te})_4]$ by dppb. The relatively slow reaction of dppb with **1** (which takes 5 h as opposed to 45 mins for dppf) potentially allows for competing formation of $[\text{Fe}_4(\text{CO})_{12}(\mu_3\text{-Te})_4]$. Alternatively, secondary rearrangements of **4** could be responsible, but all our attempts to convert **4** to **8** were unsuccessful. Similar cubane clusters were not observed as products with any of the other diphosphines used in this study.

2.4. Electrochemical studies and supporting density functional theory (DFT) calculations.

The related 50-electron clusters $[\text{Fe}_3(\text{CO})_7\text{L}_2(\mu_3\text{-Te})_2]$ ($\text{L}_2 = (\text{CO})_2$, dppm, dcpm = bis(dicyclohexylphosphino)methane) show interesting electrochemical properties [46]. These clusters exhibit two reversible reduction processes, with the diphosphine derivatives also showing quasi-reversible oxidation chemistry. Thus, a number of stable redox states are available with electron counts varying between 49 and 52, and the doubly reduced species are highly active proton reduction catalysts [47]. In order to investigate the proton reduction potential of **2-7** we carried out cyclic voltammetry (CV) studies in CH_2Cl_2 . Important features

of these studies are summarized in Table 3, with full data being given in Figs. 4-5 and S2-S3 (Supplementary Information). Cyclic voltammograms for the dppe-derivative **2** are shown in Figure 4. The electrochemical behaviour of clusters **4** (dppb) and **7** (dppbn) are very similar to that of **2**.

Each cluster undergoes a reduction between -1.61 and -1.90 V and in all cases this is irreversible at all scan rates from 0.010 to 2 Vs⁻¹. As the scan rate increases, however, a number of associated oxidation waves begin to appear, suggesting some degree of (chemical) quasi-reversibility. This suggests that the initially detected lack of reversibility at relatively slow scan rates is due to significant structural rearrangement of the cluster rather than actual decomposition. A similar behaviour has been shown by Weigand and coworkers for the clusters [Fe₂(CO)₆(μ-ECH₂CR₂CH₂E)] (E = S, Se; R = Me) with the area under the curves for the total oxidation process resulting in full chemical reversibility [48]. We have not studied this behaviour in detail but the data show that at scan rates of 0.5 V s⁻¹, a significant percentage of the parent cluster is regenerated.

The oxidation chemistry is more complex. For **2** (Fig. 4), three irreversible oxidation waves are observed at +0.36, +0.54 and +0.76 V with similar behaviour being noted for **4** and **7**. For all three clusters, the first oxidation process shows some reversibility at higher scan rates but the other two are irreversible at all scan rates. Clusters **3** (dppv) (Fig. 5), **5** (dppp) and **6** (dppf) show somewhat different oxidative behaviour to those discussed above, with each exhibiting a single irreversible oxidation peak but at similarly low potentials. The oxidation wave for **6** is especially large, which is consistent with oxidation of both the ferrocene and triiron centres.

insert Figs 4 and 5 near here

We have briefly probed the chemical oxidation of these clusters. Addition of [Cp₂Fe][PF₆] to CH₂Cl₂ solutions of **2-7** resulted in the relatively slow (1-2 h) disappearance of their characteristic carbonyl absorptions bands, which were replaced by new bands at higher frequencies; e.g. at 2078w, 2063m, 2023vs, 1985s cm⁻¹ in the case of **5**. Attempts to collect NMR spectra of the oxidized clusters were unsuccessful, suggesting that these compounds are paramagnetic, and they are therefore tentatively identified as the 51-electron clusters

$[\text{Fe}_3(\text{CO})_8(\mu_3\text{-Te})_2(\kappa^2\text{-diphosphine})]^+$ (2^+-7^+). Interestingly, exactly the same IR spectra were observed upon addition of either $\text{HBF}_4\cdot\text{Et}_2\text{O}$ or $\text{CF}_3\text{CO}_2\text{H}$ to CH_2Cl_2 solutions of **2-7** with no evidence of cluster protonation (Figure S1, Supplementary Material). This suggests, but does not prove, that under these conditions the proton is reduced by the cluster. Similar behaviour has been noted for other trinuclear clusters [49].

In order to understand the redox chemistry described above, we have carried out DFT calculations on $[\text{Fe}_3(\text{CO})_8(\mu_3\text{-Te})_2(\kappa^2\text{-dppp})]$ (**5**). The calculated HOMO and LUMO are given in Figure 6. As expected, the HOMO (Fig. 6a) is the iron-iron σ -bonding orbital localised between the two $\text{Fe}(\text{CO})_3$ subunits, a feature in common with standard [FeFe]-hydrogenase biomimics of the type $[\text{Fe}_2(\text{CO})_6(\mu\text{-EXE})]$. More surprising was the nature of the LUMO (Fig. 6b), which is delocalised across the unique iron and the two tellurium atoms, being Fe-Te anti-bonding in nature. This suggests that oxidation will result in elongation of the diiron bond, akin to the behaviour of other hydrogenase biomimics, while reduction will differ, resulting in weakening of the binding of the $\text{Fe}(\text{CO})_2(\text{diphosphine})$ subunit to the cluster core. The latter phenomenon may be related to the observed lack of reversibility upon reduction when cyclic voltammetry was carried out at relatively slow scan rates.

insert Fig. 6 near here

2.5 Electrocatalytic studies

The electrocatalytic activities of **2-7** towards H_2 production were investigated in the presence of *para*-toluenesulfonic acid (TsOH) in CH_2Cl_2 . A catalytic response was observed for **2-5** in the presence of acid and Figures 7 and S2 illustrate characteristic catalytic behaviour for clusters **3** and **5**. In all cases, as the acid concentration is increased incrementally, a significant increase in peak height is seen at the first reduction potential, indicative of hydrogen production. A second peak is also seen at slightly higher potentials and the relative size of these two peaks varies with increasing acid concentration, the second peak becoming relatively larger. The height of the oxidation peak remains unchanged upon addition of more than ten equivalents of TsOH, suggesting no significant degradation of the catalyst. At higher acid concentrations there is also the appearance of a third peak at relatively lower reduction potentials (*ca.* -1.5 V). The origin of this is not known but it could be associated with either the development of a small amount of protonated cluster or the degradation of the neutral

cluster and concomitant proton reduction by one or more of the degradation products. The electrochemical behaviour of **6-7** was also studied in CH₂Cl₂ in the presence of TsOH (Figure S6, Supplementary Material) and show similar behaviour.

insert Fig. 7 near here

Song and co-workers have reported the proton reduction ability of the related Fe₂Te₂Ni clusters [Fe₂(CO)₆(μ₃-Te)₂Ni(κ²-diphosphine)] [35]. These clusters show a quasi-reversible first reduction at around -1.6 V, followed by an irreversible second one-electron reduction at slightly higher potentials. Interestingly, all reduction processes are shifted to slightly lower potentials than the analogous selenium- and sulfur-containing clusters [35]. Addition of TsOH in MeCN to the dppv-analogue [Fe₂(CO)₆(μ₃-Te)₂Ni(κ²-dppv)] did lead to hydrogen formation at the first reduction potential. The mechanism(s) of formation of hydrogen in both **2-7** and [Fe₂(CO)₆(μ₃-Te)₂Ni(κ²-dppv)] [35] remain unknown. On the basis of the molecular orbital analysis of **5** presented herein, it would seem reasonable to suggest that proton reduction is primarily associated with the Te₂Fe(CO)₂(diphosphine) center as this is where the LUMO is localised (*vide supra*). If this is indeed the case then these catalysts (Figs. 1b-c) differ significantly from the more widely studied models (Fig. 1a) in which the LUMO is centered on the diiron centre and this is where proton reduction takes place. Further studies are required to fully elucidate the catalytic proton reduction mechanisms for these and related trinuclear clusters.

3. Summary and Conclusions

The 52-electron diphosphine-containing tellurium-capped triiron clusters [Fe₃(CO)₈(μ₃-Te)₂(κ²-diphosphine)] (diphosphine = dppe, dppv, dppb, dppp, dppf, dppbn) (**2-7**, respectively) have been prepared and characterised by, *inter alia*, IR, NMR spectroscopy, and X-ray crystallography. Complexes **2-7** contain a diphosphine-chelated Fe atom that bridges the tellurium atoms of the Fe₂Te₂ cluster core. In addition, the cubane cluster [Fe₄(CO)₁₀(μ₃-Te)₄(κ²-dppb)] (**8**) from the reaction of the precursor [Fe₃(CO)₉(μ₃-Te)₂] (**1**) with dppb. Clusters **2-7** have been examined as electrocatalysts for proton reduction. The electrocatalytic behaviour is similar for these complexes: hydrogen production occurs at the first reduction potential (ca -1.8 V) with a minor catalytic wave at more positive potential (ca -1.5V). As the

acid concentration increases, a third catalytic wave also appears at lower potential. While the electrocatalytic behaviour is superficially similar to that observed for $[\text{Fe}_2(\text{CO})_6\{\mu\text{-E}(\text{CH}_2)_3\text{E}\}]$ ($\text{E} = \text{S}, \text{Se}, \text{Te}$) complexes, computational modelling shows that the LUMO in **5** is actually centered on the Fe(diphosphine) moiety and the bridging tellurides. By extension, it is likely that the LUMOs of the diphosphine clusters **2-4** and **7** are analogous to that of **5**. Considering this, the mechanism of proton reduction is likely quite different from that observed for $[\text{Fe}_2(\text{CO})_6\{\mu\text{-E}(\text{CH}_2)_3\text{E}\}]$ being more akin to related Fe(II) complexes of the type $[\text{Fe}(\text{CO})_2(\text{diphosphine})(\text{SR})_2]$ [50-52]. The Fe-Te anti-bonding nature of the LUMO suggests that reduction may lead to scission of a Fe-Te bond, thus providing a vacant coordination site at which protonation may take place to initiate hydrogen formation. Further studies are required to confirm this.

4. Experimental

4.1. General procedures

Unless otherwise stated, purification of solvents, reactions, and manipulation of compounds were carried out under a nitrogen atmosphere using standard Schlenk techniques. Reagent grade solvents were dried by standard procedures and were freshly distilled prior to use. All chromatographic separations and ensuing work-up were carried out in air. Thin layer chromatography (TLC) was carried out on glass plates pre-coated with Merck 60 0.5 mm silica gel. All phosphines were purchased from Acros Organics Chemicals Inc. and used as received. The starting material $[\text{Fe}_3(\text{CO})_9(\mu_3\text{-Te})_2]$ (**1**) was prepared as previously reported [23]. IR spectra were recorded on Nicolet 6700 or Nicolet Avatar 360 FT-IR-spectrometers in a solution cell fitted with calcium fluoride or sodium chloride plates; subtraction of the solvent absorptions was achieved by computation. Fast atom bombardment (FAB) mass spectra were obtained on a JEOL SX-102 spectrometer using 3-nitrobenzyl alcohol as matrix and CsI as calibrant. NMR spectra were recorded on Varian Unity 500 MHz or Bruker AMX400 spectrometers. Chemical shifts were referenced to residual solvent resonances or 85% H_3PO_4 .

4.2. Synthesis of $[\text{Fe}_3(\text{CO})_8(\mu_3\text{-Te})_2(\kappa^2\text{-dppf})]$ (**2**)

A benzene solution (20 mL) of **1** (50 mg, 0.074 mmol) and dppe (30 mg, 0.074 mmol) was refluxed for 1 h. The solvent was removed under reduced pressure and the residue was chromatographed by TLC on silica gel. Elution with n-hexane/CH₂Cl₂ (7:3 v/v) developed a single band which gave [Fe₃(CO)₈(μ₃-Te)₂(κ²-dppe)] (**2**) (25 mg, 32%) as orange crystals after recrystallization from hexane/CH₂Cl₂ at 4 °C. Characterization data for **2**: IR (ν(CO), CH₂Cl₂): 2041s, 2017s, 1998vs, 1963s cm⁻¹. ¹H NMR (CDCl₃): δ 7.75-7.43 (m, 20H), 2.72-2.49 (m, 4H). ³¹P{¹H} NMR (CDCl₃): δ 69.2 (s). ESI-MS: *m/z* 1045.20 (M⁺, calc. 1045.23).

4.3. Synthesis of [Fe₃(CO)₈(μ₃-Te)₂(κ²-dppv)] (**3**)

A benzene solution (20 mL) of **1** (50 mg, 0.074 mmol) and dppv (29 mg, 0.074 mmol) was refluxed for 1.5 h. The solvent was removed under reduced pressure and the residue was chromatographed by TLC on silica gel. Elution with n-hexane/CH₂Cl₂ (7:3 v/v) developed a single band which gave [Fe₃(CO)₈(μ₃-Te)₂(κ²-dppv)] (**3**) (30 mg, 39%) as orange crystals after recrystallization from hexane/CH₂Cl₂ at 4 °C. Characterization data for **3**: IR (ν(CO), CH₂Cl₂): 2044s, 2020s, 2000vs, 1965s cm⁻¹. ¹H NMR (CDCl₃): δ 7.85 (AA'XX' m, *J* 22 Hz, 2H, HC=CH), 7.78-7.46 (m, 20H, Ph). ³¹P{¹H} NMR (CDCl₃): δ 76.7 (s). ESI-MS: *m/z* 1043.35 (M⁺, calc. 1043.21).

4.4. Synthesis of [Fe₃(CO)₈(μ₃-Te)₂(κ²-dppb)] (**4**) and [Fe₄(CO)₁₀(μ₃-Te)₄(κ²-dppb)] (**8**)

A benzene solution (20 mL) of **1** (50 mg, 0.074 mmol) and dppb (33 mg, 0.074 mmol) was refluxed for 5 h. The solvent was removed under reduced pressure and the residue was chromatographed by TLC on silica gel. Elution with n-hexane/CH₂Cl₂ (7:3 v/v) developed two bands in addition to intractable, presumably decomposed, material. The faster moving band gave [Fe₄(CO)₁₀(μ₃-Te)₄(κ²-dppb)] (**8**) (13 mg, 12%) as black crystals and the second band afforded [Fe₃(CO)₈(μ₃-Te)₂(κ²-dppb)] (**4**) (20 mg, 25%) as red crystals after recrystallization from hexane/CH₂Cl₂ at 4 °C. Characterization data for **4**: IR (ν(CO), CH₂Cl₂): 2042s, 2021s, 1998vs, 1964s cm⁻¹. ¹H NMR (CDCl₃): δ 7.70-7.67 (m, 4 H), 7.59-7.34 (m, 10H), 7.24-7.03 (m, 10H). ³¹P{¹H} NMR (CDCl₃): δ 74.2 (s). ESI-MS: *m/z* 1093.24 (M⁺, calc. 1093.27). Characterization data for **8**: IR (ν(CO), CH₂Cl₂): 2053s, 2029vs, 1977s, 1908w cm⁻¹. ¹H NMR (CDCl₃): δ 7.67-7.04 (m, 24 H). ³¹P{¹H} NMR (CDCl₃): δ 53.5 (s). ESI-MS: *m/z* 1460.33 (M⁺, calc.1460.34).

4.5. Synthesis of [Fe₃(CO)₈(μ₃-Te)₂(κ²-dppp)] (**5**)

A benzene solution (20 mL) of **1** (50 mg, 0.074 mmol) and dppp (31 mg, 0.075 mmol) was refluxed for 1 h. The solvent was removed under reduced pressure and the residue was chromatographed by TLC on silica gel. Elution with n-hexane/CH₂Cl₂ (7:3 v/v) developed a single band which gave [Fe₃(CO)₈(μ₃-Te)₂(κ²-dppp)] (**5**) (50 mg, 61%) as red crystals after recrystallization from hexane/CH₂Cl₂ at 4 °C. Characterization data for **5**: IR (ν(CO), CH₂Cl₂): 2038s, 1995vs, 1960s, 1951m cm⁻¹. ¹H NMR (CDCl₃): δ 7.67-7.33 (m, 20H), 2.43-1.83 (m, 6H). ³¹P{¹H} NMR (CDCl₃): δ 42.0 (s). ESI-MS: *m/z* 1059.13 (M⁺, calc. 1059.26).

4.6. Synthesis of [Fe₃(CO)₈(μ₃-Te)₂(κ²-dppf)] (**6**)

A benzene solution (20 mL) of **1** (100 mg, 0.148 mmol) and dppf (82 mg, 0.148 mmol) was refluxed for 45 mins. The solvent was removed under reduced pressure and the residue was chromatographed by TLC on silica gel. Elution with n-hexane/CH₂Cl₂ (3:1 v/v) developed two bands. The faster moving band gave a very dark solid, tentatively assigned as [Fe₃(CO)₉(μ₃-Te)₂(κ¹-dppfO)] (15 mg, 9%), and the second band afforded [Fe₃(CO)₈(μ₃-Te)₂(κ²-dppf)] (**6**) (60 mg, 35%) as red crystals after recrystallization from hexane/CH₂Cl₂ at 4°C. Characterization data for [Fe₃(CO)₈(μ₃-Te)₂(κ¹-dppfO)]: IR (ν(CO), CH₂Cl₂): 2053s, 2039vs, 2010vs, 1996 vs, 1964s cm⁻¹. ¹H NMR (CDCl₃): δ 8.23–7.43 (m, 20H), 4.4-4.38 (m, 4H), 3.35-3.31 (m, 4H). ³¹P{¹H} NMR (CDCl₃): δ 51.0 (s), 28.0 (s). Characterization data for **6**: IR (ν(CO), CH₂Cl₂): 2039s, 1998vs, 1963s, 1951m cm⁻¹. ¹H NMR (CDCl₃): δ 7.60-7.43 (m, 8 H), 7.4-7.43 (m, 12H), 4.47 (s, 4H), 4.38 (s, 4H). ³¹P{¹H} NMR (CDCl₃): δ 51.2 (s). ESI-MS: *m/z* 1145.47 (M⁺, calc. 1145.35).

4.7. Synthesis of [Fe₃(CO)₈(μ₃-Te)₂(κ²-dppbn)] (**7**)

A benzene solution (20 mL) of **1** (50 mg, 0.074 mmol) and dppbn (46 mg, 0.074 mmol) was refluxed for 4 h. The solvent was removed under reduced pressure and the residue was chromatographed by TLC on silica gel. Elution with n-hexane/CH₂Cl₂ (6:4 v/v) developed two bands in addition to intractable, presumably decomposed, material. The faster moving band afforded trace amounts of a dark solid, tentatively assigned as [Fe₃(CO)₉(μ₃-Te)₂(κ¹-dppbnO)], and the second band gave [Fe₃(CO)₈(μ₃-Te)₂(κ²-dppbn)] (**7**) (15 mg, 16%) as red crystals after recrystallization from hexane/CH₂Cl₂ at 4°C. Characterizing data for [Fe₃(CO)₉(μ₃-Te)₂(κ¹-dppbn)]: IR (ν(CO), CH₂Cl₂): 2063w, 2040vs, 2002s, 1970m cm⁻¹. Characterization data for **7**: IR (ν(CO), CH₂Cl₂): 2039vs, 1996vs, 1963s, 1952 cm⁻¹. ¹H NMR (CDCl₃): δ 7.85-7.33 (m, 20H), 7.14-6.71 (m, 12H). ³¹P{¹H} NMR (CDCl₃): δ 52.3 (s). ESI-MS: *m/z* 1269.25 (M⁺, calc. 1269.48).

4.8. Oxidation experiments

To CH₂Cl₂ solutions (*ca.* 1 mL) of **2-7** were added two equivalents of [Cp₂Fe][PF₆]. Over 1-2 h the four carbonyl peaks of the neutral clusters were replaced by four new carbonyl bands at higher frequencies. These changes are attributed to the formation of the 51-electron cations [Fe₃(CO)₈(μ₃-Te)₂(κ²-diphosphine)]⁺ (*vide supra*); **2**⁺ 2080w, 2063m, 2023vs, 1985s cm⁻¹; **3**⁺ 2080w, 2063m, 2023vs, 1985s cm⁻¹; **4**⁺ 2080w, 2063m, 2023vs, 1985s cm⁻¹; **5**⁺ 2078w, 2063m, 2023vs, 1985s cm⁻¹; **6**⁺ 2080w, 2062m, 2023vs, 1986s cm⁻¹ (Fig. S1, Supplementary Material); **7**⁺ 2079w, 2063m, 2023vs, 1985s cm⁻¹. Similarly, addition of two equivalents of HBF₄·Et₂O or CF₃CO₂H to **2-7** in air led to similar changes as monitored by IR spectroscopy.

4.9. X-ray structure determinations

Crystals of **4**, **5**, **7** and **8** suitable for single crystal X-ray diffraction analysis were grown by slow diffusion of hexane into CH₂Cl₂ solutions at 4 °C. A suitable crystal was selected and mounted on a SuperNova Atlas (Dual, Cu at zero) diffractometer using a nylon loop. The crystal was kept at 150 K during data collection. Using Olex2 [53], the structures of **4**, **5** and **8** were solved with the ShelXS [54] structure solution program using direct methods and refined with the ShelXL [54] refinement package using least squares minimisation. The structures of **6** and **7** were solved with the Superflip [55] structure solution program using charge flipping and refined with the Olex2 program package. Cluster **7** was refined with ShelXL using least squares minimization and **6** was refined using a refinement package with Gauss-Newton minimisation [56].

4.10. Electrochemistry

A Pine Wave Now potentiostat was used for all electrochemical measurements. Electrochemistry was carried out under solvent-saturated nitrogen in deoxygenated CH₂Cl₂ and acetonitrile solutions with 0.1 M [NBu₄][PF₆] as the supporting electrolyte. The working electrode was a 3 mm diameter glassy carbon electrode that was polished with 0.3 μm alumina slurry prior to each scan. The counter electrode was a platinum wire and the Ag/AgCl reference electrode was separated from the working electrode by a glass frit. Ferrocene was added as an internal standard and all cyclic voltammograms were referenced to the Fc⁺/Fc redox couple [57]. Catalysis studies were carried out by adding known equivalents of *p*-toluenesulfonic acid (TsOH) (Sigma-Aldrich).

4.11. DFT modeling

All calculations were performed with the hybrid DFT functional B3LYP, as implemented by the Gaussian 09 program package [58]. This functional utilizes the Becke three-parameter exchange functional (B3) [59], combined with the correlation functional of Lee, Yang and Parr (LYP) [60]. The iron atoms were described by Stuttgart–Dresden effective core potentials (ecp) and an SDD basis set, while the 6-31G(d') basis set was employed for the remaining atoms. The reported geometries were fully optimized, and the analytical second derivatives were evaluated and found to possess only positive eigenvalues. The geometry-optimized structures have been drawn with the JIMP2 molecular visualization and manipulation program [61].

Acknowledgements

AR thanks the European Commission for the award of an Erasmus Mundus pre-doctoral fellowship. GH and EN thank the Royal Society for an International Exchange Award. MGR thanks the Robert A. Welch Foundation (Grant B-1093-MGR) for financial support. Computational resources through CASCAM, which is supported by NSF (CHE-1531468), is acknowledged.

Appendix A. Supplementary data.

CCDC entries no. 1830148, 1830149, 1830150, and 1830151 contain the supplementary crystallographic data for **4**, **5**, **7** and **8**, respectively. Copies of this information may be obtained free of charge from The Director, CCDC, 12 Union Road, Cambridge, CB2 1EZ, UK (fax: +44-1223-336033; e-mail: deposit@ccdc.cam.ac.uk or www: <http://www.ccdc.cam.ac.uk>).

References:

1. Y.V. Torubaev, A.A. Pasynskii, A.V. Pavlova, M. Tauqeer, R.H. Herber, I. Nowik, I.V. Skabitskii, G.L. Denisov, V.A. Grinberg, P. Mathur, S.M. Mobin, G.K. Lahiri, J. Organomet. Chem., 777 (2015) 88-95.
2. C.M. Thomas, O. Rüdiger, T. Liu, C.E. Carson, M.B. Hall, M.Y. Darensbourg, Organometallics, 26 (2007) 3976-3984.
3. M.K. Harb, T. Niksch, J. Windhager, H. Görls, R. Holze, L.T. Lockett, N. Okumura, D.H. Evans, R.S. Glass, D.L. Lichtenberger, M. El-Khateeb, W. Weigand, Organometallics, 28 (2009) 1039-1048.
4. L.-C. Song, Q.-L. Li, Z.-H. Feng, X.-J. Sun, Z.-J. Xie, H.-B. Song, Dalton Trans., 42 (2013) 1612-1626.
5. L.-C. Song, B. Gai, H.-T. Wang, Q.-M. Hu, J. Inorg. Biochem., 103 (2009) 805-812.
6. M.K. Harb, U.-P. Apfel, J. Kübel, H. Görls, G.A.N. Felton, T. Sakamoto, D.H. Evans, R.S. Glass, D.L. Lichtenberger, M. El-Khateeb, W. Weigand, Organometallics, 28 (2009) 6666-6675.
7. M.K. Harb, H. Görls, T. Sakamoto, G.A.N. Felton, D.H. Evans, R.S. Glass, D.L. Lichtenberger, M. El-Khateeb, W. Weigand, Eur. J. Inorg. Chem., (2010) 3976-3985.
8. M.K. Harb, U.-P. Apfel, T. Sakamoto, M. El-Khateeb, W. Weigand, Eur. J. Inorg. Chem., (2011) 986-993.
9. (a) E. Garcin, X. Vernede, E.C. Hatchikian, A. Volbeda, M. Frey, J.C. Fontecilla-Camps, Structure, 7 (1999) 557-566. (b) H.S. Shafaat, O. Rüdiger, H. Ogata, W. Lubitz, Biochim. Biophys. Acta., 1827 (2013) 986-1002. (c) D. Schilter, M.J. Nilges, M. Chakrabarti, P.A. Lindahl, T.B. Rauchfuss, M. Stein, Inorg. Chem., 51 (2012) 2338-2348. (d) Z. Li, Y. Ohki, K. Tatsumi, J. Am. Chem. Soc., 127 (2005) 8950-8951.
10. R.L.O.R. Cunha, I.E. Gouvea, L. Juliano, An. Acad. Bras. Ciênc., 81 (2009) 393-407.
11. S. Chatterjee, S.K. Patel, S.M. Mobin, J. Organomet. Chem., 696 (2011) 1782-1786.
12. S. Chatterjee, S.K. Patel, V. Tirkey, S.M. Mobin, J. Organomet. Chem., 699 (2012) 12-17.
13. P. Mathur, D.K. Rai, R.S. Ji, B. Pathak, S. Boodida, S.M. Mobin, RSC Adv., 3 (2013) 26025-26034.

14. G. Hogarth, N.J. Taylor, A.J. Carty, A. Meyer, *J. Chem. Soc., Chem. Commun.*, (1988) 834-836.
15. R.D. Adams, J.E. Babin, P. Mathur, K. Natarajan, J.-G. Wang, *Inorg. Chem.*, 28 (1989) 1440-1445.
16. D. Cauzzi, C. Graiff, C. Massera, G. Predieri, A. Tiripicchio, D. Acquotti, *Dalton Trans.*, (1999) 3515-3521.
17. D. Cauzzi, C. Graiff, G. Predieri, A. Tiripicchio, C. Vignali, *Dalton Trans.*, (1999) 237-241.
18. D. Cauzzi, C. Graiff, M. Lanfranchi, G. Predieri, A. Tiripicchio, *J. Organomet. Chem.*, 536-537 (1997) 497-507.
19. D. Cauzzi, C. Graiff, M. Lanfranchi, M. Predieri, A. Tiripicchio, *Dalton Trans.*, (1995) 2321-2322.
20. P. Baistrocchi, M. Careri, D. Cauzzi, C. Graiff, M. Lanfranchi, P. Manini, G. Predieri, A. Tiripicchio, *Inorg. Chim. Acta.*, 252 (1996) 307-374.
21. P. Baistrocchi, D. Cauzzi, M. Lanfranchi, G. Predieri, A. Tiripicchio, M.T. Camellini, *Inorg. Chim. Acta.*, 235 (1995) 173-183.
22. (a) P. Mathur, S. Chatterjee, Y.V. Torubaev, *J. Clust. Sci.*, 18 (2007) 505-534. (b) M. Shieh, C.-Y. Miu, Y.-Y. Chu, C.-N. Lin, *Coord. Chem. Rev.*, 256 (2012) 637-694.
23. W. Hieber, J. Gruber, *Z. Anorg. Allg. Chem.*, 296 (1958) 91-103.
24. P.L. Stanghellini, G. Cetini, O. Gambino, R. Rossetti, *Inorg. Chim. Acta.*, 3 (1969) 651-654.
25. G. Cetini, P.L. Stanghellini, R. Rossetti, O. Gambino, *Inorg. Chim. Acta.*, 2 (1968) 427-432.
26. G. Cetini, P.L. Stanghellini, R. Rossetti, O. Gambino, *J. Organomet. Chem.*, 15 (1968) 373-381.
27. D.A. Lesch, T.B. Rauchfuss, *Inorg. Chem.*, 20 (1981) 3583-3585.
28. P. Mathur, *Adv. Organomet. Chem.*, 41 (1997) 243-314.
29. P. Mathur, I.J. Mavunkal, *J. Organomet. Chem.*, 350 (1988) 251-256.
30. P. Mathur, I.J. Mavunkal, V. Rugmini, *J. Organomet. Chem.*, 367 (1989) 243-248.
31. P. Mathur, V.D. Reddy, *J. Organomet. Chem.*, 385 (1990) 363-368.
32. (a) A.L. Arnold, R.L. Ostrander, P. Mathur, *Acta Cryst.*, C49 (1993) 1741-1743. (b) P. Mathur, A.K. Bhunia, A. Kumar, S. Chatterjee, S.M. Mobin, *Organometallics*, 21 (2002) 2215-2218.
33. S. Klose, U. Flörke, H. Egold, P. Mathur, *Organometallics*, 22 (2003) 3360-3366.

34. (a) P. Mathur, A.K. Dash, M.M. Hossain, S.B. Umbarkar, *Organometallics*, 15 (1996) 1356-1361. (b) P. Mathur, I.J. Mavunkal, V. Rugmini, *Inorg. Chem.*, 28 (1989) 3616-3618.
35. L.-C. Song, X.-J. Sun, G.-J. Jia, M.-M. Wang, H.-B. Song, *J. Organomet. Chem.*, 761 (2014) 10-19.
36. L. Duan, M. Wang, P. Li, N. Wang, F. Wang, L. Sun, *Inorg. Chim. Acta*, 362 (2009) 372-376.
37. L.-C. Song, Y.-L. Li, L. Li, Z.-C. Gu, Q.-M. Hu, *Inorg. Chem.*, 49 (21) (2010) 10174-10182.
38. L. Li, L.-C. Song, M.-M. Wang, Q.-L. Li, H.-B. Song, *Organometallics*, 30 (2011) 4899-4909.
39. (a) D.A. Lesch, T.B. Rauchfuss, *Organometallics*, 1 (1982) 499-506. (b) V.W. Day, D. A. Lesch, T.B. Rauchfuss, *J. Am. Chem. Soc.*, 104 (1982) 1290-1295.
40. (a) D.A. Lesch, T.B. Rauchfuss, *Inorg. Chem.*, 22 (1983) 1854-1857. (b) L.E.B. Jr, D.A. Lesch, T.B. Rauchfuss, *J. Organomet. Chem.*, 250 (1983) 429-438.
41. G. Gervasio, *J. Organomet. Chem.*, 441 (1992) 271-276.
42. V. Tirkey, R. Boddhula, S. Mishra, S.M. Mobin, S. Chatterjee, *J. Organomet. Chem.*, 794 (2015) 88-95.
43. K.-C. Huang, M.-H. Shieh, R.-J. Jang, S.-M. Peng, G.-H. Lee, M. Shieh, *Organometallics*, 17 (1998) 5202-5205.
44. P. Barbaro, A. Bencini, I. Bertini, F. Briganti, S. Midollini, *J. Am. Chem. Soc.*, 112 (1990) 7238-7246.
45. W. Simon, A. Wilk, B. Krebs, G. Henkel, *Angew. Chem., Int. Ed. Engl.*, 26 (1987) 1009-1010.
46. H.-O. Stephan, C. Chen, G. Henkel, K. Griesar, W. Haase, *J. Chem. Soc., Chem. Commun.*, (1993) 886-888.
47. A. Rahaman, G.C. Lisensky, M.G. Richmond, E. Nordlander, G. Hogarth, *submitted for publication*
48. R. Trautwein, L.R. Almazahreh, H. Görls, W. Weigand, *Dalton Trans.*, 44 (2015) 18780-18794.
49. N.G. Connelly, N.J. Forrow, S.A.R. Knox, K.A. Macpherson, A.G. Orpen, *J. Chem. Soc., Chem. Commun.*, (1985) 16-17.
50. S. Kaur-Ghumaan, L. Schwartz, R. Lomoth, M. Stein, S. Ott, *Angew. Chem. Int. Ed.*, 49 (2010) 8033-8036.

51. S. Ghosh, N. Hollingsworth, M. Warren, K.B. Holt, G. Hogarth, *Polyhedron*, 137 (2017) 140-146.
52. F. Ridley, S. Ghosh, G. Hogarth, N. Hollingsworth, K.B. Holt, D.G. Unwin, J. *Electroanal. Chem.*, 703 (2013) 14-22.
53. O.V. Dolomanov, L.J. Bourhis, R.J. Gildea, J.A.K. Howard, H. Puschmann, *J. Appl. Cryst.*, 42 (2009) 339-341.
54. G.M. Sheldrick, *Acta Cryst.*, A64 (2008) 112-122.
55. (a) L. Palatinus, G. Chapuis, *J. Appl. Cryst.*, 40 (2007) 786-790; (b) L. Palatinus, A.V.D. Lee, *J. Appl. Cryst.*, 41 (2008) 975-984; (c) L. Palatinus, S.J. Prathapa, S.V. Smaalen, *J. Appl. Cryst.*, 45 (2012) 575-580.
56. L.J. Bourhis, O.V. Dolomanov, R.J. Gildea, J.A.K. Howard, H. Puschmann, *J. Acta Cryst.*, 71A (2015) 59-75.
57. R.R. Gagne, C.A. Koval, G.C. Lisensky, *Inorg. Chem.*, 19 (1980) 2854-2855.
58. M.J. Frisch, *et al.*, *Gaussian 09*, Revision E.01, Gaussian, Inc., Wallingford, CT, USA, 2009.
59. A.D. Becke, *J. Chem. Phys.* 98 (1993) 5648-5652.
60. C. Lee, W. Yang and R.G. Parr, *Phys. Rev.*, B 37 (1988) 785-789.
61. (a) M.B. Hall and R.F. Fenske, *Inorg. Chem.* 11(1972) 768-775; (b) J. Manson, C.E. Webster and M.B. Hall, Texas A&M University, College Station, TX, 2006, <http://www.chem.tamu.edu/jimp2/index.html>.

Table 1. Crystallographic data for [Fe₃(CO)₈(μ₃-Te)₂(κ²-dppb)] (**4**), [Fe₃(CO)₈(μ₃-Te)₂(κ²-dppp)] (**5**), [Fe₃(CO)₈(μ₃-Te)₂(κ²-dppbn)] (**7**) and [Fe₄(CO)₁₀(μ₃-Te)₄(κ²-dppb)] (**8**).

Compound	4	5	7	8
Empirical formula	C ₃₈ H ₂₄ Fe ₃ O ₈ P ₂ Te ₂	C ₃₅ H ₂₆ Fe ₃ O ₈ P ₂ Te ₂	C ₅₂ H ₃₂ Fe ₃ O ₈ Te ₂ P ₂	C ₄₀ H ₂₄ Fe ₄ O ₁₀ P ₂ Te ₄
Formula weight	1093.26	1059.25	1269.48	1460.33
Temperature/K	150(1)	150(1)	150(1)	150(1)
Crystal system	monoclinic	triclinic	triclinic	monoclinic
Space group	P2 ₁ /n	P-1	P-1	P2 ₁ /n
a/Å	10.72662(14)	11.8170(3)	13.6004(3)	11.32884(16)
b/Å	20.3360(3)	13.1745(4)	13.7488(4)	20.9384(3)
c/Å	17.8794(3)	13.2898(4)	14.7766(3)	18.4526(3)
α/°	90	115.082(3)	78.558(2)	90
β/°	99.6852(14)	97.986(2)	75.5963(19)	92.9404(12)
γ/°	90	90.871(3)	69.768(2)	90
Volume/Å ³	3844.56(9)	1849.38(11)	2491.84(11)	4371.34(11)
Z	4	2	2	4
ρ _{calc} /cm ³	1.889	1.902	1.805	2.219
μ/mm ⁻¹	2.739	2.843	2.236	4.046
F(000)	2112.0	1024.0	1324.0	2744.0
Crystal size/mm ³	0.3 × 0.18 × 0.14	0.3 × 0.12 × 0.1	0.2 × 0.17 × 0.06	0.16 × 0.14 × 0.04
Radiation	MoKα (λ = 0.71073)			
2θ range for data collection/°	5.558 to 59.176	5.24 to 59.006	5.328 to 58.942	5.672 to 59.06
Index ranges	-14 ≤ h ≤ 14, -25 ≤ k ≤ 28, -24 ≤ l ≤ 24	-16 ≤ h ≤ 16, -18 ≤ k ≤ 18, -18 ≤ l ≤ 18	-18 ≤ h ≤ 18, -18 ≤ k ≤ 17, -18 ≤ l ≤ 18	-14 ≤ h ≤ 14, -26 ≤ k ≤ 28, -25 ≤ l ≤ 25
Reflections collected	67039	31804	42604	77288
Independent reflections	10006 [R _{int} = 0.0385, R _{sigma} = 0.0266]	9137 [R _{int} = 0.0434, R _{sigma} = 0.0425]	12203 [R _{int} = 0.0359, R _{sigma} = 0.0380]	11385 [R _{int} = 0.0314, R _{sigma} = 0.0223]
Data/restraints/parameters	10006/0/478	9137/0/451	12203/0/649	11385/0/541
Goodness-of-fit on F ²	1.065	1.066	1.042	1.110
Final R indexes [I ≥ 2σ (I)]	R ₁ = 0.0246, wR ₂ = 0.0513	R ₁ = 0.0353, wR ₂ = 0.0860	R ₁ = 0.0276, wR ₂ = 0.0555	R ₁ = 0.0267, wR ₂ = 0.0557
Final R indexes [all data]	R ₁ = 0.0335, wR ₂ = 0.0557	R ₁ = 0.0452, wR ₂ = 0.0941	R ₁ = 0.0359, wR ₂ = 0.0597	R ₁ = 0.0370, wR ₂ = 0.0607
Largest diff. peak/hole / e Å ⁻³	0.87/-0.46	1.53/-1.17	0.56/-0.76	1.91/-0.61

Table 2. Selected bond lengths (Å) and bond angles (°) for **4**, **5** and **7**

	4	5	7
Te(1) – Te(2)	3.1527(2)	3.1075(3)	3.1385(2)
Te(1) – Fe(1)	2.6135(3)	2.6536(5)	2.6591(3)
Te(1) – Fe(2)	2.5820(4)	2.5688(5)	2.5639(4)
Te(1) – Fe(3)	2.5812(4)	2.5637(5)	2.5744(4)
Te(2) – Fe(1)	2.6490(3)	2.6543(5)	2.6724(4)
Te(2) – Fe(2)	2.5696(4)	2.5702(5)	2.5709(3)
Te(2) – Fe(3)	2.5877(4)	2.5734(5)	2.5634(4)
Fe(1) – P(1)	2.2373(6)	2.2590(9)	2.2582(6)
Fe(1) – P(2)	2.2082(6)	2.2419(9)	2.2579(7)
Fe(2) – Fe(3)	2.5832(5)	2.5903(7)	2.6011(5)
P(1) – Fe(1) – Te(2)	174.40(2)	164.54(3)	90.604(19)
P(2) – Fe(1) – Te(1)	170.72(2)	171.87(3)	100.061(19)
P(2) – Fe(1) – Te(2)	97.161(18)	100.22(3)	170.47(2)
P(2) – Fe(1) – P(1)	87.25(2)	94.12(3)	97.29(2)
Te(1) – Fe(1) – Te(2)	73.606(9)	71.668(13)	72.125(9)
P(1) – Fe(1) – Te(1)	101.908(18)	93.89(3)	162.64(2)

Table 3. Reduction and oxidation potentials for clusters **2-7**

Complexes	1 st reduction	1 st oxidation	2 nd oxidation	3 rd oxidation
[Fe ₃ (CO) ₈ (μ ₃ -Te) ₂ (κ ² -dppe)] (2)	-1.81	+0.36	+0.54	+0.76
[Fe ₃ (CO) ₈ (μ ₃ -Te) ₂ (κ ² -dppv)] (3)	-1.84	+0.35		
[Fe ₃ (CO) ₈ (μ ₃ -Te) ₂ (κ ² -dppb)] (4)	-1.81	+0.33	+0.51	+0.74
[Fe ₃ (CO) ₈ (μ ₃ -Te) ₂ (κ ² -dppp)] (5)	-1.90	+0.28		
[Fe ₃ (CO) ₈ (μ ₃ -Te) ₂ (κ ² -dppf)] (6)	-1.61	+0.29 ^a		
[Fe ₃ (CO) ₈ (μ ₃ -Te) ₂ (κ ² -dppbn)] (7)	-1.65	+0.07	+0.40	+0.74

^a Larger peak current might indicate a 2e⁻ oxidation

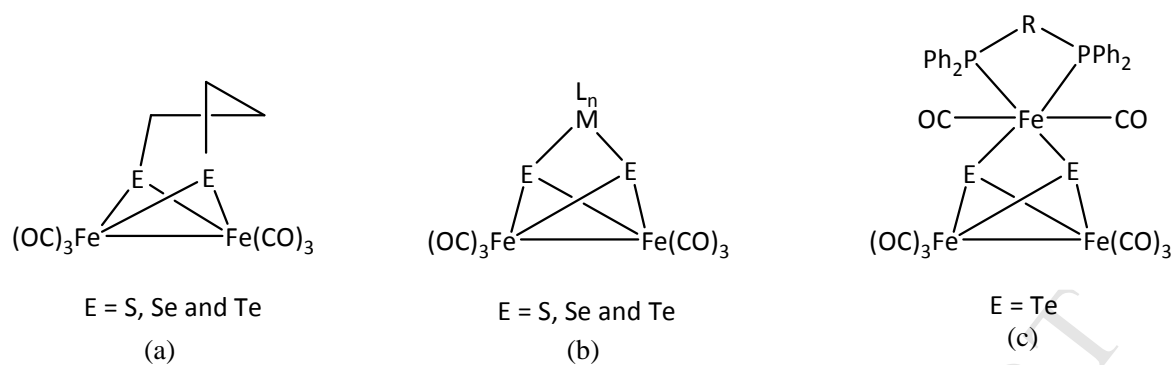


Fig. 1. (a) Biomimics of [FeFe]-hydrogenases, (b) metal-substituted biomimics of [FeFe]-hydrogenases, (c) general structure of clusters reported in this article.

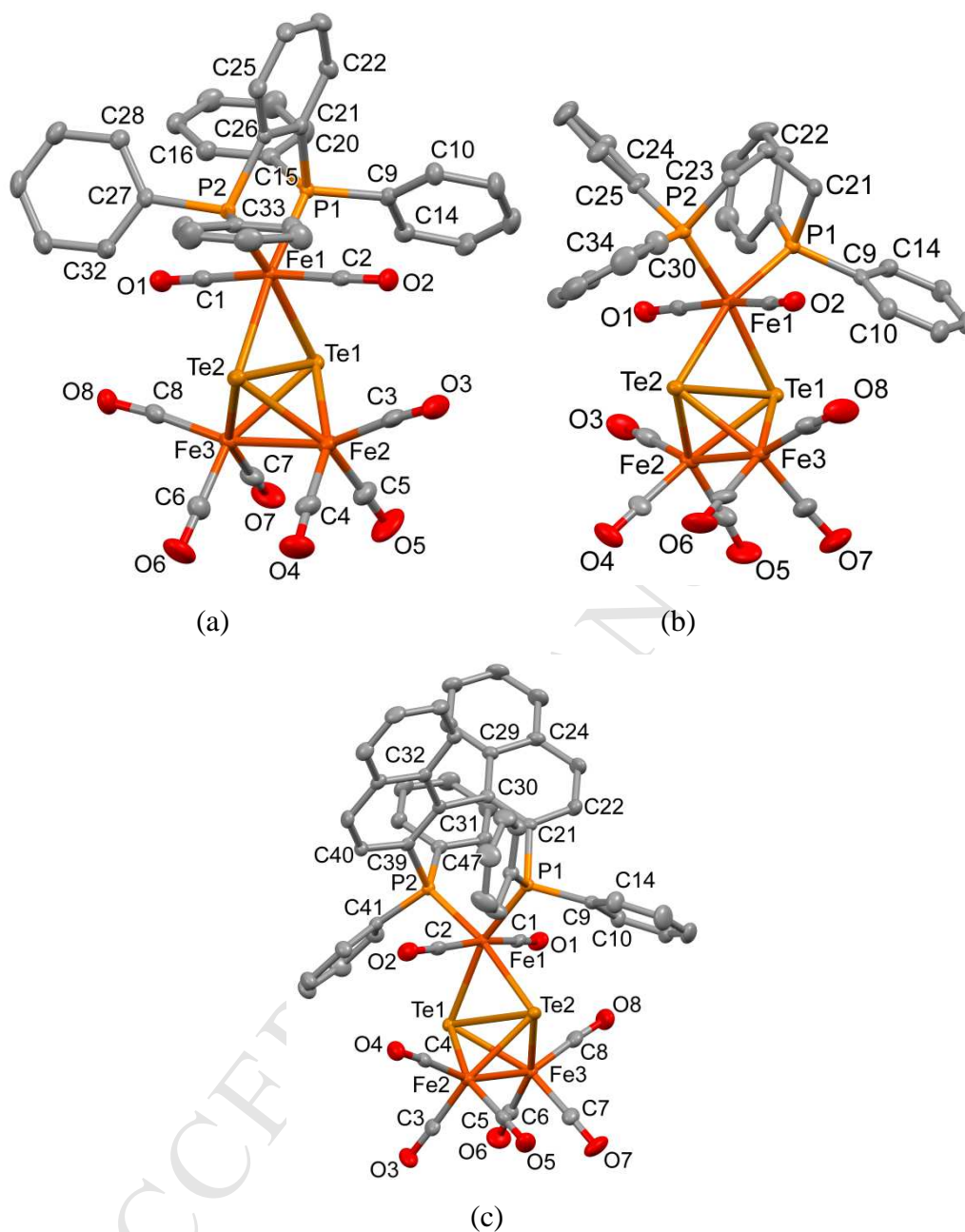


Fig. 2. Molecular structures of (a) $[\text{Fe}_3(\text{CO})_8(\mu_3\text{-Te})_2(\kappa^2\text{-dppb})]$ (**4**), (b) $[\text{Fe}_3(\text{CO})_8(\mu_3\text{-Te})_2(\kappa^2\text{-dppp})]$ (**5**) and (c) $[\text{Fe}_3(\text{CO})_8(\mu_3\text{-Te})_2(\kappa^2\text{-dppbn})]$ (**7**) showing the atom numbering scheme. Thermal ellipsoids are drawn at the 50% probability level (hydrogen atoms omitted for clarity).

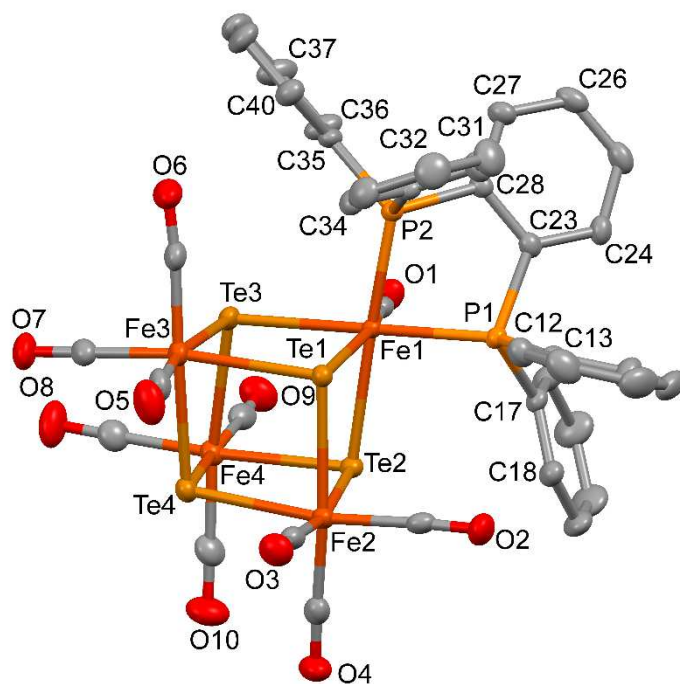


Fig.3. Molecular structure of $[\text{Fe}_4(\text{CO})_{10}(\mu_3\text{-Te}_4)(\kappa^2\text{-dppb})]$ (**8**) showing the atom numbering scheme. Thermal ellipsoids are drawn at the 50% probability level (hydrogen atoms omitted for clarity).

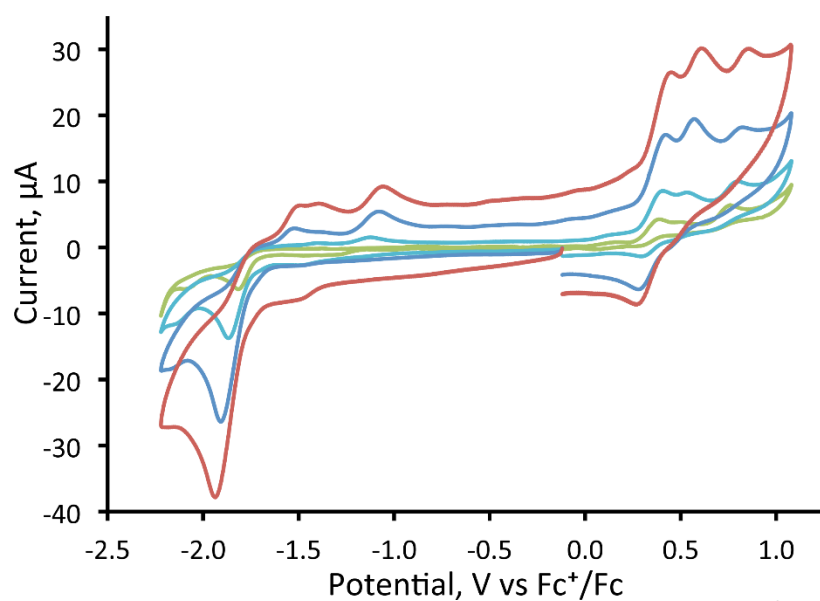


Fig. 4. Cyclic voltammetry of 1 mM $[\text{Fe}_3(\text{CO})_8(\mu_3\text{-Te})_2(\kappa^2\text{-dppe})]$ (**2**) in CH_2Cl_2 (supporting electrolyte $[\text{NBu}_4][\text{PF}_6]$); peak heights increase with the scan rate of 0.010, 0.050, 0.250, and 0.500 Vs^{-1} ; glassy carbon electrode; potential vs. Fc^+/Fc .

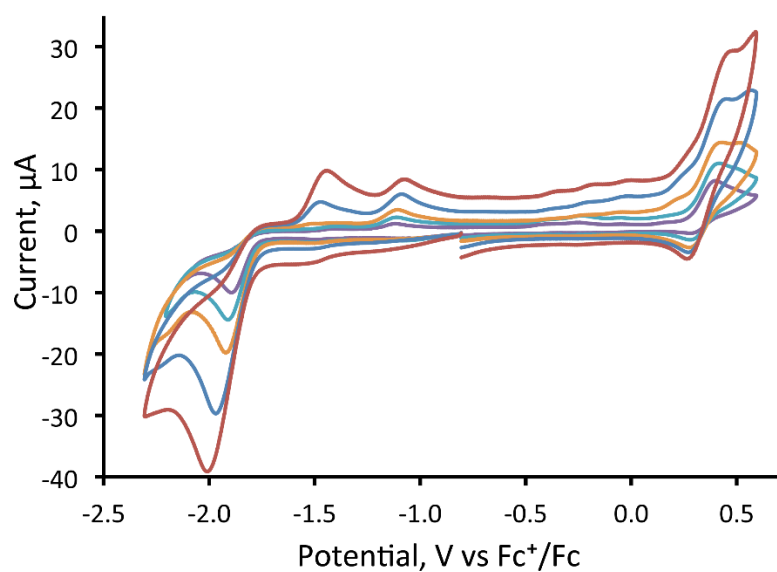


Fig. 5. Cyclic voltammetry of 1 mM $[\text{Fe}_3(\text{CO})_8(\mu_3\text{-Te})_2(\kappa^2\text{-dppv})]$ (**3**) in CH_2Cl_2 (supporting electrolyte $[\text{NBu}_4][\text{PF}_6]$, peak heights increase with the scan rate 0.025, 0.050, 0.100, 0.250 and 0.500 V s^{-1} ; glassy carbon electrode, potential vs. Fc^+/Fc).

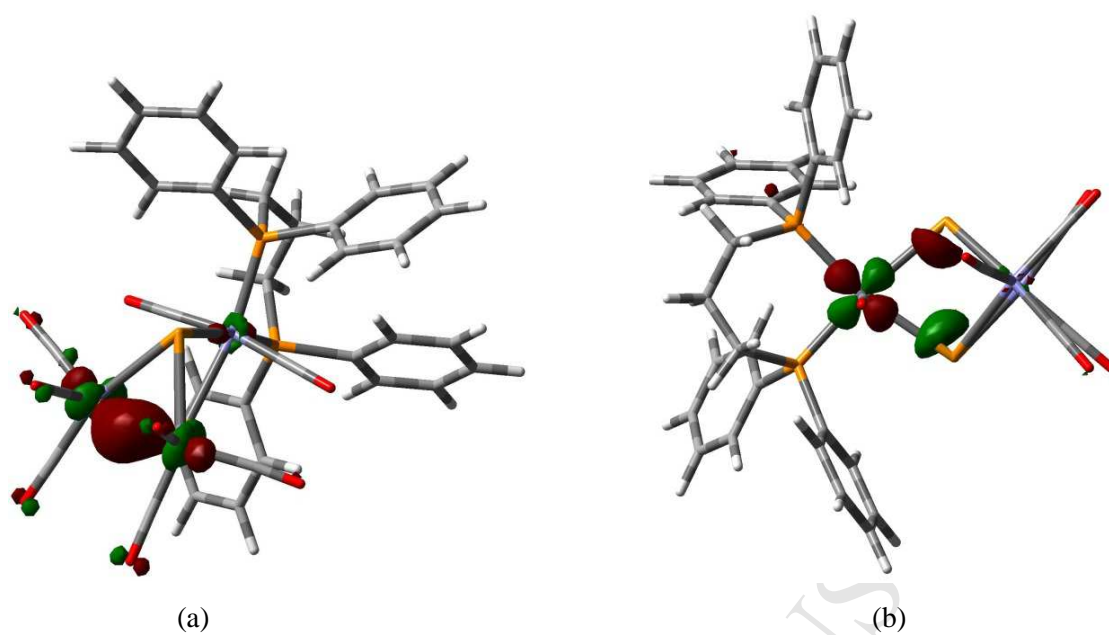


Fig. 6. (a) HOMO and (b) LUMO in $[\text{Fe}_3(\text{CO})_8(\mu_3\text{-Te})_2(\kappa^2\text{-dppp})]$ (5) as calculated by DFT. Both orbital plots were printed at an isovalue of 0.055.

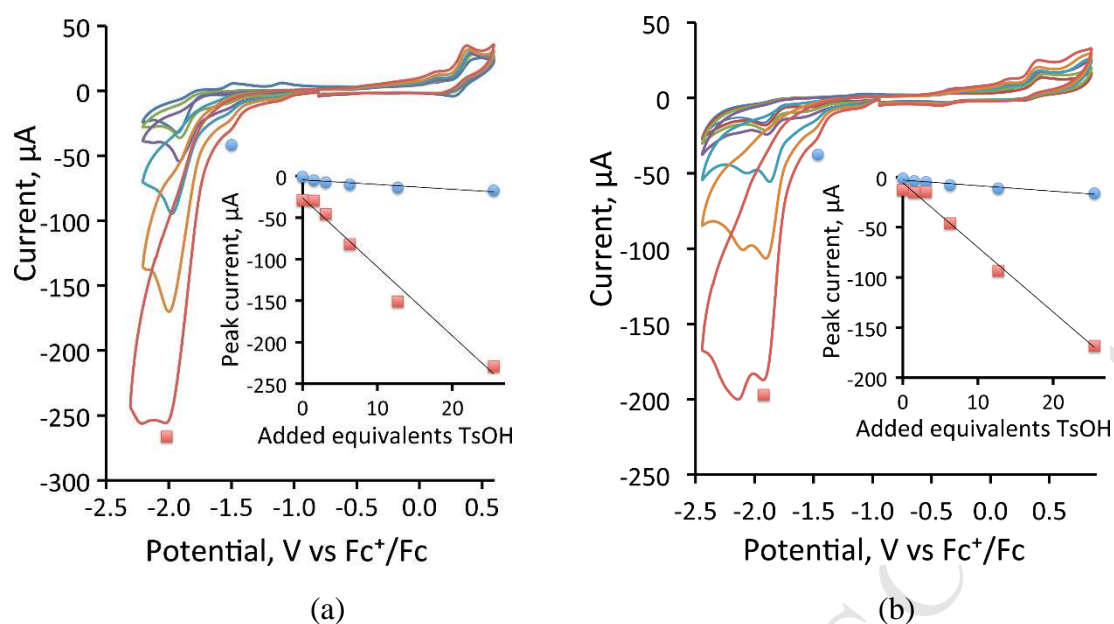
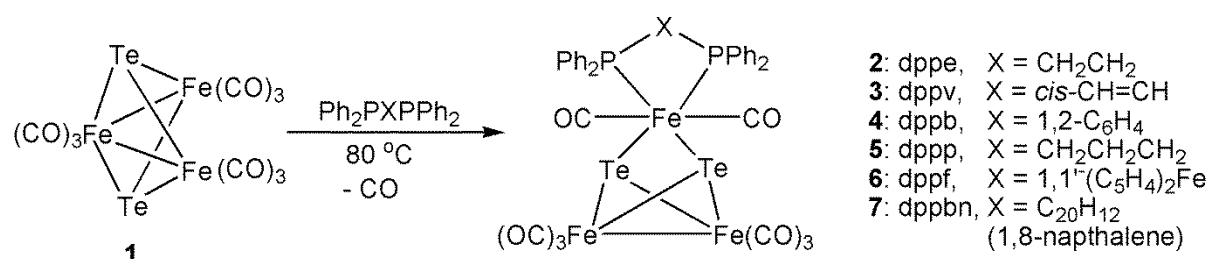


Fig. 7. Cyclic voltammetry of 1 mM $[\text{Fe}_3(\text{CO})_8(\mu_3\text{-Te})_2(\kappa^2\text{-dppv})]$ (**3**) (a) and 1 mM $[\text{Fe}_3(\text{CO})_8(\mu_3\text{-Te})_2(\kappa^2\text{-dppv})]$ (**5**) (b) in the absence and presence of 1–25 molar equivalents of *p*-TsOH (supporting electrolyte $[\text{NBu}_4][\text{PF}_6]$, scan rate 0.2 Vs^{-1} , glassy carbon electrode, potential vs. Fc^+/Fc). Peak heights increase with 0, 1.5, 3.1, 6.3, 12.7, and 25.5 equivalents. Dilution corrections have been made so that the figures represent the results at constant volume. The inset shows the observed peak current at the initial reduction (circle) and at a new reduction (square) as TsOH is added.



Scheme 1

Highlights

- 52-electron $[\text{Fe}_3(\text{CO})_9(\mu_3\text{-Te})_2(\text{k}^2\text{-diphosphine})]$ clusters have been prepared.
- All clusters display similar electrochemical behaviour (cyclic voltammetry).
- All clusters are electrocatalysts for proton reduction.